Mode characteristics of nano-width rectangle resonator

Ke Yao (姚 轲)[1], Guoying Feng (冯国英)[1*], and Shouhuan Zhou (周寿桓)[1,2*]

[1] *Department of Opt-Electronics, Sichuan University, Chengdu 610064, China*

[2] *North China Research Institute of Electro-Optics, Beijing 100015, China*

[*] *Corresponding author: guoing_feng@scu.edu.cn; [**] corresponding author: zhousf@scu.edu.cn*

Received October 19, 2013; accepted December 31, 2013; posted online , 2014

A new method based on Maxwell's equations, ABCD ray matrices, and total internal reflection is proposed to theoretically analyze the characteristics of eigenmodes confined in nano-width rectangle resonators. Using this method, mode wavelengths and indices of transverse and longitudinal modes are obtained. Another method based on the finite difference time domain technique and Padé approximation is used to numerically calculate resonant wavelengths, mode field distributions and quality factors. The results of two methods show that the resonant wavelengths obtained from both methods are very close, and the maximum relative error is less than 2%. The mode indices of transverse and longitudinal modes obtained agree well with mode field distribution patterns calculated by finite difference time domain techniques.

OCIS codes: 230.5750, 230.3390, 230.7370.

doi: 10.3788/COL201412.022303.

Optical micro-resonators have attracted great attention for their advantages of ultrasmall cavity volume and high quality factors (Q-factors) and applications in photonic integrated circuits such as optical add-drop filters, sensors and microlasers of ultra-low-threshold operation[1−7]. Recently, nanocrystalline Cr^{2+}-doped ZnSe nanowires have been fabricated using femtosecond laser ablation in our lab and mid-infrared oscillation at 2194 nm has been established[8]. The nanowires were usually 30-120 nm in diameter and several tens of micrometers in length. What is more interesting is the phenomenon that Cr^{2+}-doped ZnSe nanowires laser showed a 150-nm shift to shorter wavelengths in comparison with the bands of microsized powder random laser. All these experiments activate researchers to investigate the operating mechanism and mode characteristics of microcavites. Microcavities shaped with circular[9], ring[10,11], square-shaped[12], and equilateral resonator[13,14] have been studied. Especially for microcavity lasers with equilateral resonator, a great deal of research work has been devoted including eigenmodes[15−17], mode distributions[18,19], and Q-factors[20−22].

In this letter, the three-dimensional (3D) nanowire was simplified as two-dimensional (2D) nano-width rectangle resonator (NWRR). A new method based on Maxwell's equations and ABCD ray matrices combined with total internal reflection (TIR) was proposed by studying the modes characteristics of NWRR. Analyses of mode wavelengths and mode indices of transverse modes and longitudinal modes confined in the NWRR were presented. In order to verify the analysis, we calculated the mode frequencies, Q-factors, and mode field distributions using finite-difference time-domain (FDTD) technique and Padé approximation. NWRR with widths of 0.1, 0.3, and 0.5 μm and length of 5 μm was selected to analyze and calculate. The results show that the resonant wavelengths and mode indices obtained from analytical results agree well with those obtained from FDTD results. The maximum relative error of wavelengths is less than 2%. For the NWRRs with widths of 0.1 and 0.3 μm, only fundamental modes exist. When the width is increased to 0.5 μm, higher order modes appear. For the fundamental modes, the interval number of peaks in mode field distribution patterns is exactly equal to the indices of longitudinal mode and patterns are distributed on the centerline. For higher-order mode, patterns shift deviating from centerline and keep centrosymmetric along the centerline. Also the results that Q-factors increased with widths were proved. The unique properties of NWRR make it is very attractive to apply it to micro-devices with some special arrangements.

To analyze the mode characteristics for NWRR, the x-z coordinate systems were chosen, as shown in Fig. 2, with the z-axis parallel with the long side and the x-axis parallel with the short side. The length of NWRR is l, the width is d, and the refractive index is n. Based on the Maxwell's equations, the time-independent wave equation is obtained as

$$\nabla^2\vec{E} + n^2k_0^2\vec{E} = 0, \tag{1}$$

where $k_0 = 2\pi/\lambda_0$ is the free space wave number, λ_0 is the mode wavelength. For NWRR, the modes consist of TE and TM modes. We begin with the derivation of the TE modes. Only the following field components are nonzero: H_z, H_x, and E_y. Using Maxwell's equation, H_z and H_x can be expressed in terms of E_y. E_y component is obtained as a solution of Eq. (1), which is

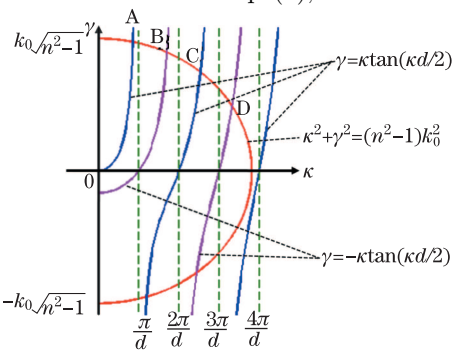

Fig. 1. (Color online) Graphical solution of the eigenvalue equation for TE mode. Blue lines and pink lines are for even and odd TE modes, respectively.

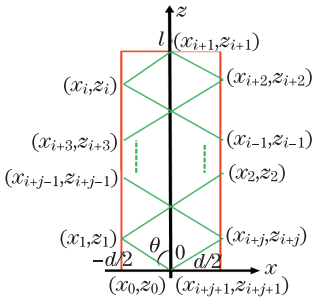

Fig. 2. (Color online) Scheme of light propagation in NWRRs.

$$\frac{\partial^2 E_y}{\partial x^2} + (n^2 k_0^2 - \beta^2) E_y = 0, \tag{2}$$

where β is the propagation constant along the z-axis. The solution of Eq. (2) is always complex. Here we simplify the mode analysis by considering the even and odd solutions of eigenvalue equation separately.

First we consider the even TE modes. A general solution of Eq. (2) is of the form

$$E_y = \begin{cases} A\cos(\kappa x), & \text{for} \quad |x| \leqslant d/2 \\ Be^{[-\gamma(|x|-d/2)]}, & \text{for} \quad |x| > d/2 \end{cases}. \tag{3}$$

From Eqs. (2) and (3), we can get

$$\kappa^2 + \gamma^2 = (n^2 - 1)k_0^2. \tag{4}$$

Considering the continuity of E_y and $\partial E_y/\partial x$ at the interface of $|x|$=d/2, we obtain the eigenvalue equation:

$$\gamma = \kappa \tan(\kappa d/2). \tag{5}$$

A similar analysis can be carried out for the odd TE modes with the only difference that $\cos(\kappa x)$ in Eq. (3) is replaced by $\sin(\kappa x)$. The application of the boundary conditions now yields

$$\gamma = -\kappa \cot(\kappa d/2). \tag{6}$$

Equation (4) describes a circle in the $\kappa - \gamma$ plane, and its intersection with the curves obtained using Eqs. (5) and (6) yields κ_p and γ_p values for the p-th TE mode. Multiple solutions occur because of the periodic nature of trigonometric functions. The number of allowed modes can be determined by noting that a solution is no longer bounded if $\gamma \leqslant 0$ since it leads to an exponential growth of field distribution E_y. The cut-off condition is thus determined by $\gamma = 0$. Setting $\gamma = 0$ in Eqs. (4)–(6), the number of TE mode p can be obtained as

$$p = \frac{k_0 d\sqrt{n^2 - 1}}{\pi} = \frac{2d\sqrt{n^2 - 1}}{\lambda}. \tag{7}$$

We draw the curves in the $\kappa - \gamma$ plane which are obtained using Eqs. (4)–(6), as shown in Fig. 1. The solutions are obtained at the intersections among the curves, which are the values corresponding with the intersection points A, B, C, and D. From it, we can obtain the number of mode solutions is mainly determined by the refractive index n, the width d, and the wavelength λ_0 which is characterized by k_0. For decreasing the wavelength, this point moves to larger value of κ and as a result more mode solutions occur. Similar analysis can be carried out for the dependence of mode solutions number on n and d. The figure also shows the lowest order even TE mode can propagate at arbitrarily small frequency. It is the only mode that is never cut off.

The TM modes are obtained by setting H_z=0. The only nonvanishing filed components are E_z, E_x, and H_y. The two electric components can be expressed in terms of H_y component. The H_y component is obtained as a solution of the reduced wave equation:

$$\frac{\partial^2 H_y}{\partial x^2} + (n^2 k_0^2 - \beta^2) H_y = 0. \tag{8}$$

The continuity of H_y and $\partial H_y/\partial x$ at the interface of $|x| = d/2$ requires that B=Acos(κd/2). With the equation E_z=$-i/(n2\omega\varepsilon_0)\cdot(\partial H_y/\partial x)$, following expression can be obtained as

$$E_z = \begin{cases} \dfrac{iA\kappa}{n^2\omega\varepsilon_0}\sin(\kappa x), & \text{for} \quad |x| \leqslant d/2 \\ \dfrac{iB\gamma}{\omega\varepsilon_0} e^{[-\gamma(|x|-d/2)]}, & \text{for} \quad |x| > d/2 \end{cases}. \tag{9}$$

The eigenvalue equation is obtained from the requirement that E_z remain continuous at $|x| = d/2$. We obtain the eigenvalue equation:

$$\tan\frac{\kappa d}{2} = n^2\frac{\gamma}{\kappa}. \tag{10}$$

The analysis of odd TM modes is similar except that $\sin(\kappa x)$ in Eq. (9) is replaced with –$\cos(\kappa x)$. Then we obtain

$$\cot\frac{\kappa d}{2} = -n^2\frac{\gamma}{\kappa}. \tag{11}$$

In NWRR, mode field is confined in resonator by total internal reflection (TIR) which requires the incident angles to be greater than or equal to the critical angle. Based on the light ray concept, we can obtain

$$\min(\theta_c, \pi/2 - \theta_c) \leqslant \arctan\frac{\kappa}{\beta} \leqslant \max(\theta_c, \pi/2 - \theta_c), \tag{12}$$

where function min() and max() are solving the minimum value and maximum value in bracket, respectively. θ_c is the critical angle, whose value is arcsin($1/n$). With the equation $\kappa^2 = n^2 k_0^2 - \beta^2$, we can obtain

$$\min(\theta_c, \pi/2 - \theta_c) \leqslant \arctan\frac{\kappa}{\sqrt{n^2 k_0^2 - \kappa^2}} \leqslant \max(\theta_c, \pi/2 - \theta_c). \tag{13}$$

Here, we assume that θ_c and $\pi/2 - \theta_c$ yield the inequality $\pi/2 - \theta_c > \theta_c$, which is always true in experiments. Furthermore, we can get the requirement for TIR:

$$k_0 \leqslant \kappa \leqslant k_0\sqrt{n^2 - 1}. \tag{14}$$

For analysis of longitudinal mode, ABCD ray matrices were used to calculate the indices of longitudinal mode. The scheme of light propagation in NWRR was shown

in Fig. 2. The light propagates from (x_0,z_0), and after a round trip of passing the points $(x_1,\ z_1)$, $(x_2,\ z_2)$,$\cdots$, $(x_{i-1},\ z_{i-1})$, $(x_i,\ z_i)$, $(x_{i+1},\ z_{i+1})$, $(x_{i+2},\ z_{i+2})$, $(x_{i+3},\ z_{i+3})$,$\cdots$, $(x_{i+j-1},\ z_{i+j-1})$, $(x_i,\ z_j)$, it returns $(x_{i+j+1},\ z_{i+j+1})$. θ is the degree between the direction of light propagation and the z direction.

With the ABCD matrices, the relationship between neighboring points of TIR on the long side of NWRR satisfies

$$\begin{bmatrix} x_{m+1} \\ z_{m+1} \end{bmatrix} = \begin{bmatrix} A & B \\ C & D \end{bmatrix} \begin{bmatrix} x_m \\ z_m \end{bmatrix}, \tag{15}$$

where $m = 1, 2, \cdots,\ i,\ i+2,\ i+3,\ \cdots,\ i+j,\ i$ and j is the times of total internal reflection at the interface of $|x| = d/2$ of light propagating along the z direction, respectively. From the figure, based on the light ray concept, we can obtain

$$M_m = \begin{bmatrix} A & B \\ C & D \end{bmatrix} = \begin{bmatrix} -1 & 0 \\ 2\cot\theta \times (-1)^m & 1 \end{bmatrix}. \tag{16}$$

$$\begin{bmatrix} x_i \\ z_i \end{bmatrix} = M_{i-1} \cdots M_2 M_1 \begin{bmatrix} x_1 \\ z_1 \end{bmatrix}. \tag{17}$$

$$\begin{bmatrix} x_{i+j} \\ z_{i+j} \end{bmatrix} = M_{i+j-1} \cdots M_{i+3} M_{i+2} \begin{bmatrix} x_{i+2} \\ z_{i+2} \end{bmatrix}. \tag{18}$$

Based on Eqs. (16)–(18), if we set the point $(x_0,\ z_0)$, then we can obtain the point $(x_{i+j+1},\ z_{i+j+1})$ after a round trip. To form constructive interference, x_{i+j+1} is required to be equal to x_0.

$$x_1 = -d/2, \qquad z_1 = (x_0 + d/2)\cot\theta, \tag{19}$$

$$x_{i+2} = -x_i, \qquad z_{i+2} = 2l - d\cot\theta - z_i, \tag{20}$$

$$x_{i+j+1} = sign(x_{i+j})(d/2 - z_{i+j}\tan\theta), \quad z_{i+j+1} = 0. \tag{21}$$

Our goal is to solve the $\lambda_{p,m}$ where subscripts p and m are the transverse mode index and longitudinal mode index of resonant wavelength, respectively. In the part above, κ_p and β_p are obtained, where subscript p is the p-th solution of equations. Based on the approximation θ_p=arctan(κ_p/β_p), θ_p will be solved. Then we can calculate the optical length l_p in NWRR and the times ξ_p of TIR on sides of $|x| = d/2$ which can be solved.

To obtain constructive interference, the phase delay should be an integral multiple of 2π. Then we can obtain the $\lambda_{p,m}$ as following expression for TE mode:

$$\frac{2\pi n l_p}{\lambda_{p,m}} + \xi_p\varphi_{p1} + 2\varphi_{p2} = 2m\pi, \tag{22}$$

$$\lambda_{p,m} = \frac{2\pi n l_p}{2m\pi - \xi_p\varphi_{p1} - 2\varphi_{p2}}, \tag{23}$$

where φ_{p1} and φ_{p2} are the phase mutation of TIR on long side and short side of NWRR, respectively, which obey the following expression:

$$\varphi_{p1} = -2\arctan(\sqrt{\cos^2\theta_p - 1/n^2}/\sin\theta_p), \tag{24}$$

$$\varphi_{p2} = -2\arctan(\sqrt{\sin^2\theta_p - 1/n^2}/\cos\theta_p). \tag{25}$$

Here length l of NWRR is 5 μm, refractive index n is 3.2, and width d is varying among 0.1, 0.3, and 0.5 μm. The mode indices and wavelengths obtained are shown in first column and third column in Tables 1, 2, and 3. From the tables, when the widths are 0.1 and 0.3 μm, only fundamental modes exist. While with width increasing to 0.5 μm, higher-order modes begin to appear. The number of transverse modes N is the sum of TE even mode number $N_{\rm even}$ and odd mode number $N_{\rm odd}$, $N = N_{\rm even} + N_{\rm odd}$. Take the TE mode for example, and set λ_0 to be 1.5 μm. When width d is 0.1 μm, the value of $2(n^2-1)^{1/2}d/\lambda$ is 0.405. Based on the graphical solution of eigenvalue Eqs. (5) and (6), we can get $N_{\rm even}$ =1, $N_{\rm odd}$ =0 and N =1. Only fundamental modes exist. Similar calculations can be conducted to widths

Table 1. Resonant Wavelengths and *Q*-Factors for NWRR with the Width of 0.1 μm for TE Mode

TE Mode	λ (μm) (FDTD)	λ (μm) (Analysis)	Relative Error	*Q*-Factor
$TE_{0,16}$	1.2543	1.2515	0.223%	39.87
$TE_{0,15}$	1.3107	1.3146	0.296%	39.12
$TE_{0,14}$	1.3725	1.3740	0.109%	34.86
$TE_{0,13}$	1.4404	1.4390	0.097%	30.86
$TE_{0,12}$	1.5197	1.5190	0.046%	28.73
$TE_{0,11}$	1.6132	1.6087	0.279%	21.6
$TE_{0,10}$	1.7134	1.7077	0.333%	19.01
$TE_{0,9}$	1.8332	1.8290	0.229%	17.77

Table 2. Resonant Wavelengths and *Q*-Factors for NWRR with the Width of 0.3 μm for TE Mode

TE Mode	λ (μm) (FDTD)	λ (μm) (Analysis)	Relative Error	*Q*-Factor
$TE_{0,23}$	1.2395	1.2602	1.670%	84.93
$TE_{0,22}$	1.2882	1.3056	1.350%	77.63
$TE_{0,21}$	1.3409	1.3544	1.812%	71.03
$TE_{0,20}$	1.3907	1.4070	1.001%	67.66
$TE_{0,19}$	1.4564	1.4639	0.515%	64.77
$TE_{0,18}$	1.5197	1.5255	0.184%	62.67
$TE_{0,17}$	1.5936	1.5926	0.063%	61.52
$TE_{0,16}$	1.6750	1.6658	0.549%	55.28
$TE_{0,15}$	1.7594	1.7461	0.756%	54.13
$TE_{0,14}$	1.8592	1.8345	1.329%	50.75

Table 3. Resonant Wavelengths and Q-Factors for NWRR with the Width of 0.5 μm for TE Mode

TE Mode	λ (μm) (FDTD)	λ (μm) (Analysis)	Relative Error	Q-Factor
$TE_{2,27}$	1.3160	1.3102	0.441%	82.60
$TE_{1,26}$	1.3710	1.3788	0.569%	95.97
$TE_{2,26}$	1.4278	1.4110	1.177%	65.57
$TE_{1,25}$	1.4928	1.4891	0.248%	85.89
$TE_{0,18}$	1.5604	1.5337	1.711%	64.74
$TE_{1,23}$	1.6384	1.6530	0.891%	62.93

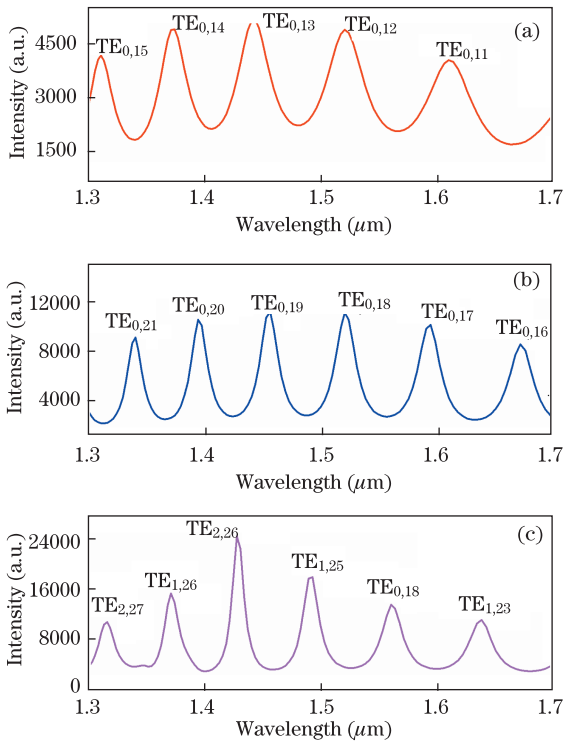

Fig. 3. (Color online) TE mode spectral distribution of NWRRs with width of (a) 0.1, (b) 0.3, and (c) 0.5 μm, respectively.

of 0.3 and 0.5 μm, and the vualues of $2(n^2-1)^{1/2}d/\lambda$ are 1.216 and 2.026, respectively. After an exact solution of equations, we can obtain for $d = 0.3$ μm, $N_{\text{enen}} = 1$, $N_{\text{odd}} = 0$, $N = 1$ and for $d = 0.5$ μm, $N_{\text{enen}} = 2$, $N_{\text{odd}} = 1$, $N = 3$. What is more, in Tables 1 and 2, the indices of fundamental longitudinal mode are varying continuously while in Table 3 the indices are complex. To some extent, this is similar to the traditional laser resonator.

The mode wavelengths, Q-factors and mode field distributions are numerically calculated by FDTD technique[23] and Padé approximation[24]. Parameters of NWRRs are the same with those of theoretically analyses. The intensity, wavelength and pulse time of pumping sources are the same. The spectral distributions of different widths for TE mode are plotted in Fig. 3. The transverse and longitudinal mode indices are obtained by comparing with the analytical wavelength in Eq. (23). From Fig. 3, we can see the spectral intensity and Q-factor in Fig. 3(c) are obviously larger than

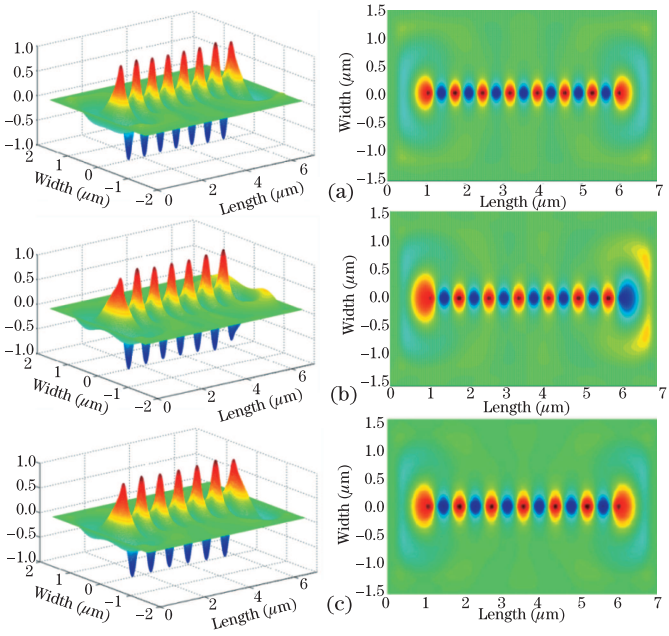

Fig. 4. (Color online) TE mode field distribution of resonant wavelengths of NWRRs with width of 0.1 μm. (a) $TE_{0,14}$ mode ($\lambda = 1.3725$ μm); (b) $TE_{0,13}$ mode (λ=1.4404 μm); (c) $TE_{0,12}$ mode (λ=1.5197 μm).

those in Figs. 3(a) and (b), which indicates that the losses for larger width of NWRR are smaller. Here, the Q-factor is defined as $Q = f_{p,m}/\Delta f$, where $f_{p,m}$ is the frequency corresponding with the $\lambda_{p,m}$ and Δf is the –3 dB bandwidth. The mode wavelength $\lambda_{p,m}$ is from the local maximum.

We summarized the relationships of mode indices, wavelengths and Q-factors obtained from FDTD and analysis results for TE mode as shown in Tables 1, 2, and 3. The first, second, and third columns show the mode indices, wavelengths calculated by FDTD technique, and wavelengths obtained by analysis results, respectively. The Q-factors in forth column are calculated from spectra. In Table 1, it can be seen that mode wavelengths obtained from FDTD technique and analytical results are very close and the relative error is small. It is worthy noticing that the relative errors around 1.5 μm are smaller than others, which is because the wavelength is set to 1.5 μm in analyses. Same conclusions can be obtained in Tables 2 and 3. In general, the maximum relative error is less than 2% and with the width decreasing, Q-factors thereupon decrease. This is because the energy of evanescent wave is more when the width is smaller, which makes the Q-factors decrease.

Furthermore, we calculated the mode distributions of resonant wavelengths for different widths by FDTD technique shown in Figs. 4–6. Based on the analyses above, we know that Figs. 4 and 5 show the distributions of fundamental modes and it can be seen that the patterns are mainly distributed on the centerline of NWRRs. And the longitudinal indices of fundamental modes are just equal to the interval number of peaks in mode field distributions. Take Fig. 4(a) for an example, the interval number is 14, and the longitudinal index is 14. Same results can be obtained in Figs. 4(b)–(d) and Fig. 5. The conclusions indicate that the theoretically analytical re-

sults agree well with the numerically calculated results. In Fig. 6, the modes consist of higher-order modes and fundamental modes, and the mode distributions are obviously different. Figures 6(a)–(d) show the distribution of

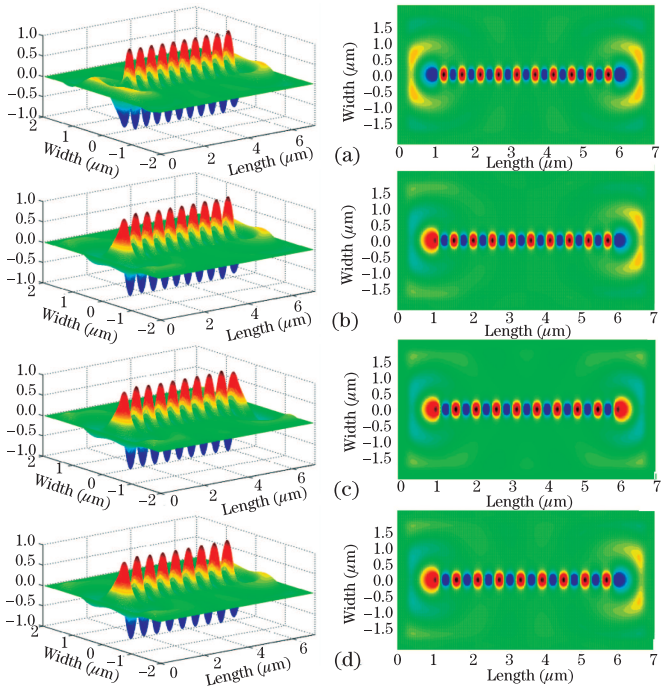

Fig. 5. (Color online) TE mode field distribution of resonant wavelengths of NWRRs with width being 0.3 μm. (a) $TE_{0,20}$ mode (λ=1.3944 μm); (b) $TE_{0,19}$ mode (λ=1.4564 μm); (c) $TE_{0,18}$ mode (λ=1.5197 μm); (d) $TE_{0,17}$ mode (λ=1.5936 μm).

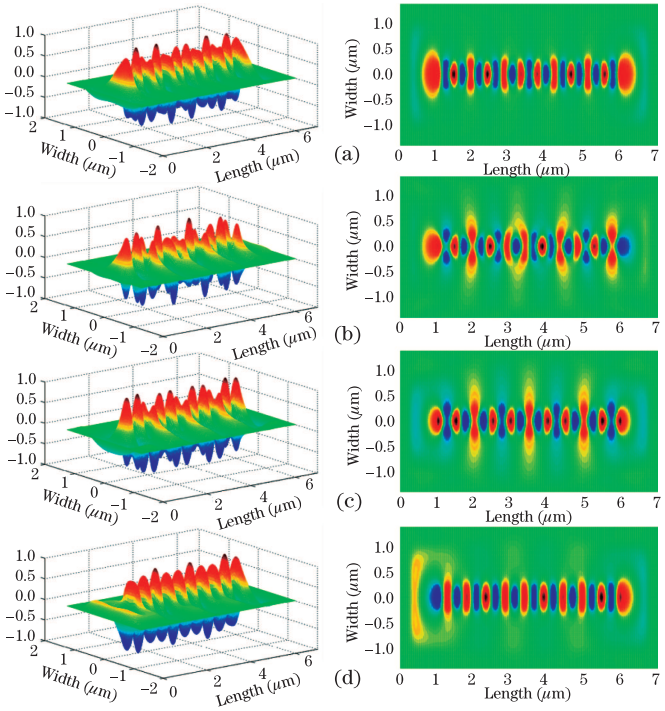

Fig. 6. (Color online) TE mode field distribution of resonant wavelengths of NWRRs with width being 0.5 μm. (a) $TE_{1,26}$ mode (λ=1.3710 μm); (b) $TE_{2,26}$ mode (λ = 1.4728 μm); (c) $TE_{1,25}$ mode (λ=1.4928 μm); (d) $TE_{0,18}$ mode (λ=1.5604 μm).

$TE_{1,26}$, $TE_{2,26}$, $TE_{1,25}$, $TE_{0,18}$ mode, respectively. From it, we can conclude that with transverse mode order increasing, some peaks of mode patterns shift deviating from centerline but keep centrosymmetric along the centerline. This can be explained by ray optics qualitatively. When transverse mode index gets larger, θ thereupon increases, and as a result the patterns shift deviating from centerline.

In conclusion, we analyze the mode characteristics of NWRRs with the new method based on Maxwell's equations and ABCD ray matrices combined with total internal reflection (TIR). We derive the wavefunctions, eigenvalues, ABCD matrices and TIR, and solve the mode wavelengths and mode indices of transverse modes and longitudinal modes. In order to verify the analysis, we calculate the mode frequencies, Q-factors, and mode field distributions using FDTD technique and Padé approximation. The NWRRs with widths of 0.1, 0.3, and 0.5 μm and length of 5 μm are theoretically analyzed and numerically calculated. The results show that the resonant wavelengths and mode indices obtained from analytical results agree well with those obtained from FDTD results. The maximum relative error of wavelengths is less than 2%. For the NWRRs with widths of 0.1 and 0.3 μm, only fundamental modes exist. When the width increases to 0.5 μm, higher-order modes appear. For the fundamental modes, the interval number of peaks in mode field distribution patterns is exactly equal to the index of longitudinal mode, and the mode distribution patterns distribute on the centerline of NWRRs. For higher order modes, the patterns shift deviating from centerline, but keep centrosymmetric. The unique properties of NWRR make it is very attractive to be applied to micro-devices with some special arrangements.

This work was supported by the Major Program of National Natural Science Foundation of China (No. 60890200) and the National Natural Science Foundation of China (No. 10976017).

References

1. Y. Panitchob, G. S. Murugan, M. Zervas, P. Horak, S. Berneschi, S. Pelli, G. Nunzi Conti, and J. Wilkinson, Opt. Express **16,** 11066 (2008).
2. G. T. Paloczi, Y. Huang, A. Yariv, and S. Mookherjea, Opt. Express **11,** 2666 (2003).
3. X. Duan, Y. Huang, R. Agarwal, and C. M. Lieber, Nature **421,** 241 (2003).
4. M. A. Zimmler, T. Voss, C. Ronning, and F. Capasso, Appl. Phys. Lett. **94,** 241120 (2009).
5. Q. Yang, X. Jiang, X. Guo, Y. Chen, and L. Tong, Appl. Phys. Lett. **94,** 101108 (2009).
6. C. Yin, J. Gu, M. Li, Y. Song, Chin. Opt. Lett. **11,** 082302 (2013)
7. F. Xu, L. Lu, W. L?, B. Yu, Chin. Opt. Lett. **11,** 082802 (2013)
8. G. Feng, C. Yang, and S. Zhou, Nano Lett. **13,** 272 (2012).
9. D. Rafizadeh, J. Zhang, S. Hagness, A. Taflove, K. Stair, S. Ho, and R. Tiberio, Opt. Lett. **22,** 1244 (1997).
10. B. E. Little, J. Foresi, G. Steinmeyer, E. Thoen, S. Chu, H. Haus, E. Ippen, L. Kimerling, and W. Greene, IEEE Photon. Technol. Lett. **10,** 549 (1998).

11. B. Little, S. Chu, W. Pan, and Y. Kokubun, IEEE Photon. Technol. Lett. **12,** 32 (2000).
12. A. Poon, F. Courvoisier, and R. Chang, Opt. Lett. **26,** 632 (2001).
13. W. Yan, Z. Guo, N. Zhu, and Y. Jiang, Opt. Express **21,** 16536 (2013).
14. Y. Huang, W. Guo, and Q. Wang, Appl. Phys. Lett. **77,** 3511 (2000).
15. J. H. Wu and A. Liu, Opt. Lett. **31,** 1720 (2006).
16. Y. Huang, W. Guo, and Q. Wang, IEEE J. Quantum. Electron. **37,** 100 (2001).
17. G. M. Wysin, J. Opt. Soc. Am. B **23,** 1586 (2006).
18. Y. Huang, Q. Lu, W. Guo, and L. Yu, IEEE Proc. Optoelectron. **151,** 202 (2004).
19. Y. Yang, Y. Huang, K. Che, S. Wang, Y.-H. Hu, and Y. Du, IEEE J. Sel. Top. Quantum **15,** 879 (2009).
20. Y. Huang, W. Guo, and L. Yan, Chin. Phys. Lett. **19,** 674 (2002).
21. W. Guo, W. Li, and Y. Huang, IEEE Microw. Wirel. Co. **11,** 223 (2001).
22. W. Guo, Y. Huang, and Q. Wang, IEEE Photon. Technol. Lett. **12,** 813 (2000).
23. K. Yao, G. Feng, L. Yang, J. Yi, Y. Song, and S. Zhou, Chin. Opt. Lett. **10,** 082901 (2012).
24. S. Dey and R. Mittra, IEEE Microw. Guid. Wav. Lett. **8,** 415 (1998).